

Minimal mechanism for flocking in phoretically interacting active particles

Arvin Gopal Subramaniam,^{1,2,*} Sagarika Adhikary,^{1,2,†} and Rajesh Singh^{1,2,‡}

¹*Department of Physics, Indian Institute of Technology Madras, Chennai 600036, India*

²*Center for Soft and Biological Matter, IIT Madras, Chennai 600036, India*

Collective motion as a flock is a widely observed phenomenon in active matter systems. We report a flocking transition mechanism in a system of chemically interacting active colloidal particles sustained purely by chemo-repulsive torques at low to medium densities. The basic requirements to maintain the polar liquid flock are excluded volume repulsions and deterministic long-ranged net repulsive torques. The mechanism we report requires that the time scale individual colloids move a unit length to be dominant with respect to the time they deterministically sense chemicals. This can be equivalently interpreted as pair colloids sliding a minimal unit length before deterministically rotating due to chemical interactions. Switching on the translational repulsive forces renders the flock a crystalline structure. We complement these results with an analysis of a continuum hydrodynamic model, with the transition corresponding to destabilization of the flocking state.

I. INTRODUCTION

The collective swarming behaviour of interacting agents - also called flocking [1] - has been a topic of sustained interest in the field of non-equilibrium statistical physics. Flocking is also a ubiquitous phenomena in the natural world, widely reported in groups of animals such as birds, fish, and mammals [2]. Paradigmatic models that incorporate local alignment interactions to study flocking have been extensively studied [1, 3–5] and continue to be investigated [6–9]. In the Vicsek model [3], local alignment interactions among the individual agents can lead to transition from a disordered state to one with large-scale, coordinated movement. The flocking transition in Vicsek-like models with short-range interactions has been widely studied, and traveling density bands are observed at the onset of transition [4, 5, 10, 11].

The possibility of attaining an emergent global polar order (flocking) arising purely out of dynamical particle-based models, without any explicit alignment interaction, is a subject of recent interest [12]. Studies on these include those studying the interplay between non-equilibrium phase separation [13] and other collective dynamics [14–17], those that study the effect of velocity alignment interactions [18–20], models incorporating attractive interactions [21, 22], history-dependence [23, 24], and those that exclusively study the effect of repulsive forces and torques [25, 26]. Though various possible mechanisms deviating from the Vicsek-like phenomenology have been established, the explicit relevance of the separate force and torque contributions have not been established. For instance, migrating cells that display a global polarity have been known to display chemo-tactic attractive interactions in addition to (among others) either a contact “inhibited” or “attracted” locomotion - akin to a long-ranged torque of either repulsive or attractive nature [22, 27, 28]. Thus, open questions remain on

the minimal ingredients and mechanism at play arising from the rotational and translational components separately.

In this paper, we report a minimal mechanism for the formation of polar liquids where colliding pair particles have to sufficiently slowly rotate in response to chemical gradients before moving a unit distance upon collision. The basic ingredients that are *sufficient* to produce such a flock are thus (i) short-ranged excluded volume repulsion, and (ii) long-ranged (chemo) repulsive torques. There is no need for any additional (chemo)repulsive translational forces between the particles, nor is there a requisite role for noise in destabilizing the flock. Furthermore, the incorporation of long-ranged translational chemo-repulsive forces between the particles induces instead a crystalline flock (with regular lattice spacing). Our work thus adds insights to investigations on attaining a global polar order via dynamical mechanisms (i.e. without any explicit alignment interaction) by providing a minimal mechanism, both for flock formation and destabilization, that, to our best knowledge, has not been reported elsewhere.

The remainder of the paper is organized as follows. In section II, we describe our model to study phoretic (chemical) interactions of active particles. In section III, we present our results from particle-based numerical simulations by mapping phase diagrams and describing the properties of the two distinct flocking states. The two distinct flocking states are termed as: CLF (Chemorepulsive Liquid Flocks), and CCF (Chemorepulsive Crystalline Flocks). Chemorepulsive torques between the particles, which turn them away from each other [15, 23, 26], are essential for the formation of both CLF and CCF states. For the formation of CCF, we require both chemorepulsive force as well as chemorepulsive torques. See below for details. Then, we complement the results from particle-based simulation with a stability analysis of a continuum description in section IV. Finally, we conclude in section V by summarizing our main results and comparing it with existing literature, along with suggesting directions for future investigations.

* Contributed equally; ph22d800@smail.iitm.ac.in

† Contributed equally; a.sagarika@physics.iitm.ac.in

‡ rsingh@physics.iitm.ac.in

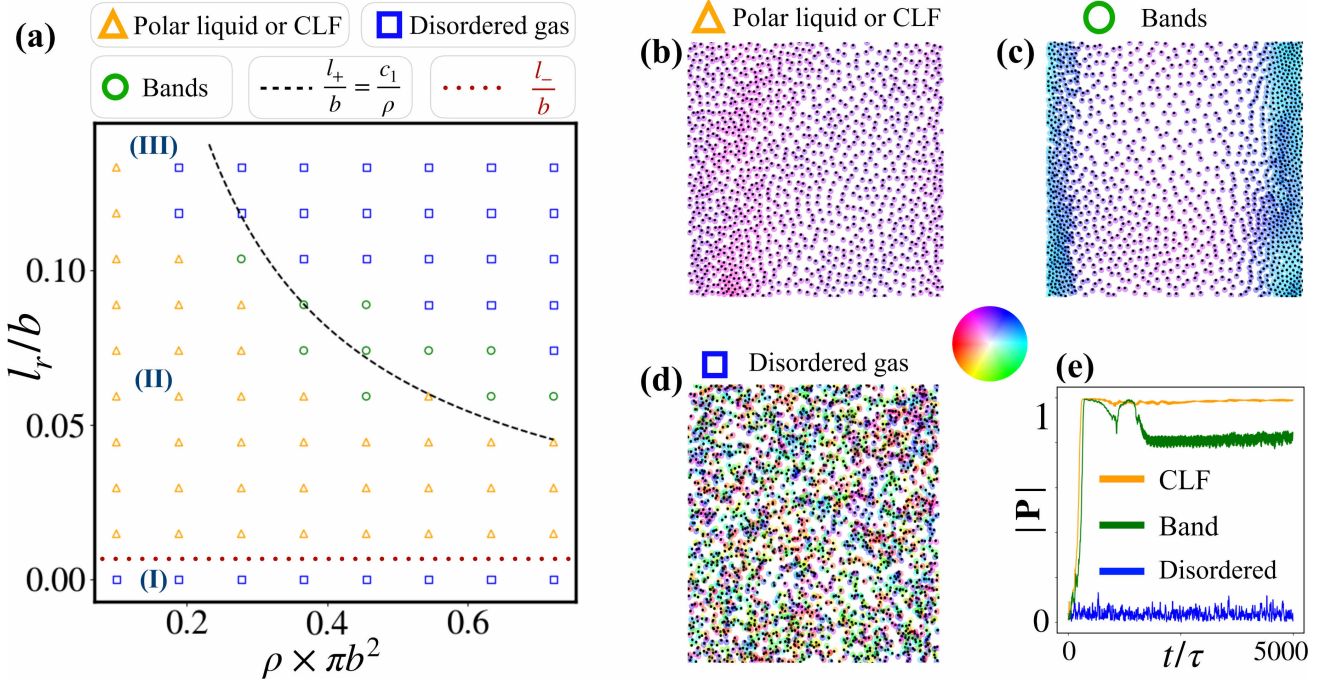


FIG. 1. Polar liquid flocks for $\chi_t = 0$. (a) Phase diagram in the $(\rho, l_r/b)$ plane. Here, l_-/b is annotated as a dotted red line, while the density dependent l_+/b in dashed black line. Symbols here and throughout the paper denoting a flock (yellow triangle), bands (green circles), and disordered (blue squares). These are distinguished with different values of polar order parameter \mathbf{P} : flock ($\mathbf{P} > 0.9$), bands ($0.1 < \mathbf{P} < 0.9$) and disordered ($\mathbf{P} < 0.1$). Marked (I)-(III) scenario and transition lines (black and red) are described in the schematic shown in Fig. 2. Snapshots of the respective phases are shown in (b)-(d) respectively (color coding for orientation of each particle is in middle panel). (e) The evolution of the polarization is displayed for the corresponding states (similarly colored). See Movie I [29] for dynamics to obtain CLF starting with a disordered state.

II. MODEL

We consider a set of N chemically interacting polar colloids. We model the i th active particle as a colloid particle centered at $\mathbf{r}_i = (x_i, y_i)$, confined to move in two-dimensions, which self-propels with a speed v_0 , along the directions $\mathbf{e}_i = (\cos \theta_i, \sin \theta_i)$. Here $i = 1, 2, 3, \dots, N$ and θ_i is the angle made by the orientation \mathbf{e}_i with respect to the positive x -axis. The orientation \mathbf{e}_i of the i th particle, given in terms of the angle θ_i , changes due to coupling its dynamics to the dynamics of a phoretic (scalar) field c , as we describe below. The position \mathbf{r}_i and orientation \mathbf{e}_i of the i th particle is updated as:

$$\dot{\mathbf{r}}_i = \mathbf{V}_i, \quad \dot{\mathbf{e}}_i = \boldsymbol{\Omega}_i \times \mathbf{e}_i, \quad (1)$$

Here, the translational velocity \mathbf{V}_i and angular velocity $\boldsymbol{\Omega}_i$ of the i th particle are given as:

$$\mathbf{V}_i = v_0 \mathbf{e}_i + \chi_t \mathbf{J}_i + \mu \mathbf{F}_i + \boldsymbol{\eta}_i^t, \quad (2a)$$

$$\boldsymbol{\Omega}_i = \chi_r (\mathbf{e}_i \times \mathbf{J}_i) + \boldsymbol{\eta}_i^r. \quad (2b)$$

Here v_0 is the self-propulsion speed of an isolated active particle. The term \mathbf{J}_i is chemical flux on the location of the i th particle, which gives the inter-particle interaction (of chemical origin). The phoretic flux is given as: $\mathbf{J}_i(t) = -[\nabla c(\mathbf{r}, t)]_{\mathbf{r}=\mathbf{r}_i}$, where $c(\mathbf{r}, t)$ is the concentration

of the chemicals (e.g filled micelles in an oil-emulsion system [23, 30]). The concentration field evolves in time as:

$$D_c \nabla^2 c(\mathbf{r}, t) + \sum_{i=1}^N c_0 \delta(\mathbf{r} - \mathbf{r}_i) = 0. \quad (3)$$

Here, D_c is the diffusion coefficient and c_0 is emission constant of the chemical. We assume the limit in which chemical field leads to instantaneous interactions between the colloidal surfaces [31–34]. The solution of the Eq.3 can be used to compute \mathbf{J}_i as:

$$\mathbf{J}_i = \frac{c_0}{4\pi D_c} \sum_{\substack{j=1 \\ i \neq j}}^N \frac{\mathbf{r}_{ij}}{r_{ij}^3} \quad (4)$$

Here, $r_{ij} = |\mathbf{r}_{ij}|$, with $\mathbf{r}_{ij} = \mathbf{r}_i - \mathbf{r}_j$. The term proportional to χ_r in Eq.(2) drives orientational changes (turning away from each other if $\chi_r > 0$) through interparticle chemical interactions. In this paper, we only consider case of $\chi_r > 0$ when particles turn away from each other due to chemical interactions [23, 24]. Similarly, the term proportional to χ_t ensures repulsion in the positional dynamics if $\chi_t > 0$. Here, both χ_r and χ_t are positive (unless otherwise stated) and the system is said to be *chemo-repulsive*.

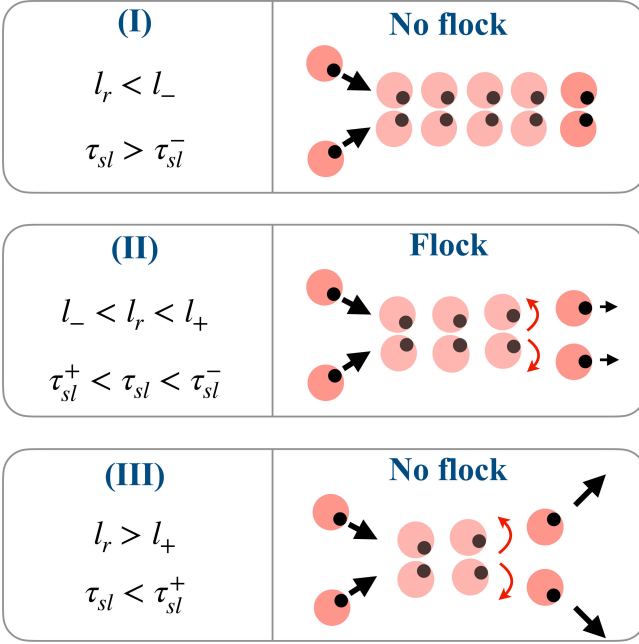


FIG. 2. Schematic of the mechanism for formation of fluid flocks. *Top-to-bottom*: Series of scenarios depicted corresponding to parameters choices labelled in Fig.1a. Top (I) and bottom (III) panels show scenarios where the chemical response is either too slow or too quick, such that a stable flock cannot be formed. The middle panel (II) shows the pair collision mechanism that would produce a flock if the time scale follow: $\tau_{sl}^+ < \tau_{sl} < \tau_{sl}^-$. See text for details.

In Eqs.(1)-(2), to preclude overlap of the particles, there is a force on the particles: $\mathbf{F}_i = -\nabla_i \mathcal{U}$, while, $\mathcal{U} = \sum_{i < j} \mathcal{U}^e(\mathbf{r}_i, \mathbf{r}_j)$. With b as the colloidal radius, we choose \mathcal{U}^e to be of the form: $\mathcal{U}^e = \kappa(r_{ij} - 2b)^2$ if $r_{ij} < 2b$, while it vanishes otherwise. Here, κ is a constant. In Eq.2, $\boldsymbol{\eta}_i^t$ and $\boldsymbol{\eta}_i^r$ are white noises with zero mean and no temporal correlation. The variance of noises $\boldsymbol{\eta}_i^t$ and $\boldsymbol{\eta}_i^r$, are respectively, $2D_t$ and $2D_r$. These noises terms are included for the sake of completion and to demonstrate that our results are robust against weak fluctuations. In this paper, the fluctuations are set to be negligibly small to emphasize that flocks can be formed and destroyed by deterministic causes [35]. Simulation details along with the full set of parameters used to generate each figure is given in the Appendix A. The dimensions of chemical concentration is: $[c] = [\text{L}^{-3}]$, and chemical flux are $[\mathbf{J}] = [\text{L}^{-4}]$. Thus, the dimensions of parameters are $[\chi_r] = [\text{L}^4 \text{T}^{-1}]$ and $[\chi_t] = [\text{L}^5 \text{T}^{-1}]$.

III. RESULTS

We first summarize our main results for the case of $\chi_t = 0$ (no chemorepulsive forces between the particles). In particular, we report here polar fluids that are obtained due to chemo-repulsive torques alone ($\chi_r > 0$).

See Fig.1. These flocks are obtained only if pair colloids move at least a distance (l_{sl}^+ , defined later) before deterministically rotating away due to sensing of chemical gradients. The schematic of the mechanism for polar fluids that we report is presented in Fig. 2. For $\chi_t > 0$, we obtain crystalline flocks that are obtained via a combination of repulsive torques and forces (Fig. 3(c)). We also find these crystalline flocks for (a narrow range of) *attractive* forces (Fig. 3(b)). In this paper, we denote the former as “Chemorepulsive Liquid Flocks” (CLF), and the later as “Chemorepulsive Crystalline Flocks” (CCF).

A. CLFs via long-ranged repulsive torques

We first consider the case of $\chi_t = 0$, thus repulsions are only short-ranged that avoid overlap of the particles in the system via \mathbf{F}_i . The phase diagram delimiting polar flocks (or CLF), bands, and disordered states are shown in Figure 1(a). The states are delimited via the mean global polarization of the system at the steady state, $\langle |\mathbf{P}| \rangle_{ss}$, where the polarization \mathbf{P} is defined as the average of sum of the orientation of all the particles:

$$\mathbf{P} = \frac{1}{N} \sum_{i=1}^N \mathbf{e}_i. \quad (5)$$

On the (ρ, χ_r) plane (Fig. 1(a)), we see that low density flocks are sustained, that are eventually destabilized at sufficiently high repulsion and densities. These flocks have evidently a liquid-like spatial structure (Fig. 1(b); see also Fig. 3(d)) [25, 36, 37]. The density field ρ is thus not homogeneous across the system (see Fig. 1(c)). We note that $\tau = b/v_0$ is the propulsion time scale. In addition, we define $\tau_r = b^4/\chi_r$, which sets the time scale for deterministic rotation of the particle due to phoretic interactions.

The phenomenology of the CLF can also be understood by a comparison of the relevant length scales of the problem. First, we write down natural length scales that arise out of the equations of motion (1). They are:

$$l_r = \frac{b\tau}{\tau_r} = \frac{\chi_r}{b^2 v_0}, \quad l_t = \frac{\chi_t}{b^3 v_0}. \quad (6)$$

Here, l_r is a deterministic length scale constructed by multiplying the radius b of the particle with the ratio of propulsion time scale τ and time scale τ_r which controls rotations of the particle orientations from chemical interactions between particles. On the other hand, l_t is a deterministic translational length, which measures ratio of translation due to chemical interactions between particles and one-body propulsion. From the phase diagram, we see that there are separate length scales that arise as a consequence of the collective many-body dynamics. To this end, let us construct a *sliding* time scale τ_{sl} and length scale l_{sl} . The time-scale τ_{sl} is time during which pair colloids slide a distance l_{sl} whilst rotating away. Similarly, l_{sl} represents the typical length the

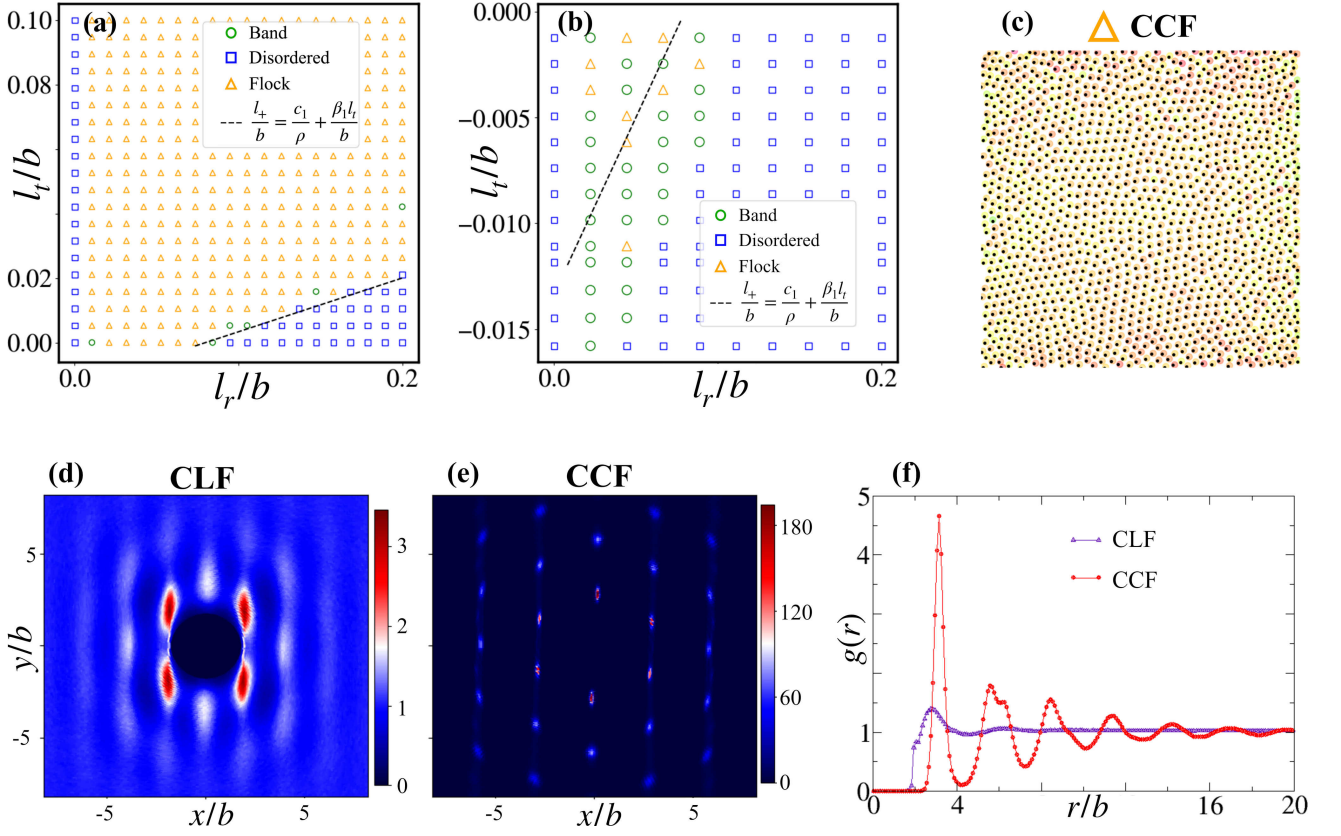


FIG. 3. (a) Phase diagram in the $(l_r/b, l_t/b)$ plane for the case of $\chi_t > 0$. Dashed line refers to lower bound on χ_r , solid line for lower bound on χ_r from Eq. (8). (b) Similar phase diagram for the case of $\chi_t < 0$ (extension of (a)). The transition line is extrapolated from (3)(a). (c) Shows a snapshot of the CCF phase (same color scheme as in Fig (1)). See Movie II [29] for dynamics to obtain CCF starting with a disordered state. (d) and (e) compare $g(r, \phi)$ for the case of the CLF and the CCF. In (f), a comparison of the flocking phase, for CLF and CCF, is shown for the pair correlation $g(r)$.

pair colloids would co-move upon collision before rotating away. The sliding time τ_{sl} and length l_{sl} can be written as:

$$\tau_{sl} = \frac{b^2}{v_0 l_r}, \quad l_{sl} = v_0 \tau_{sl} = \frac{v_0 b^4}{\chi_r}. \quad (7)$$

We next use these to understand the mechanism of formation of CLF.

Let us denote l_- as the smallest value of l_r to sustain the CLF (corresponding to the lowest transition line in Fig.1a), and l_+ as the largest value of l_r above which the CLF is not sustained. l_+ is density dependent, as we describe below. The mechanism for the CLF can then be understood as a competition between l_r and l_+ , l_- ; this is illustrated in Fig. 2 (annotated accordingly in the phase diagram of Fig.1(a)). Equivalently, the mechanism can be understood in terms of sliding time scale τ_{sl} along with τ_{sl}^- and τ_{sl}^+ . We now use the schematic of Fig. 2 to explain a series of transitions from disorder-to-order-to-disordered phases. When $l_r < l_-$ (corresponding to $\tau_{sl} > \tau_{sl}^-$), we have a *sub-deterministic* sensing of the chemicals; here the orientational changes of the colloids are too slow compared to the free movement time,

pair colloids slide excessively long, hence local polar order cannot be sustained. See panel (I) of Fig. 2. Increasing l_r , in the regime of $l_- < l_r < l_+$ (equivalently $\tau_{sl}^+ < \tau_{sl} < \tau_{sl}^-$), we have that the chemical response time fast enough such that local polar order is sustained, but still sufficiently slow such that the forward-backward symmetry at the pair collision level is broken. See panel (II) of Fig. 2. Finally for $l_r > l_+$ (equivalently $\tau_{sl} < \tau_{sl}^+$), the chemical response is sufficiently quick such that there is no symmetry breaking at the pair collision level. See panel (III) of Fig. 2. We note that from simulations at $\rho \approx 0.1$, we find these values to be $l_{sl}^+ \sim 8.3b$ and $l_{sl}^- \sim 100b$. Here $l_{sl}^+ = v_0 \tau_{sl}^+$ and $l_{sl}^- = v_0 \tau_{sl}^-$ (note that in our notation choice $l_{sl}^- > l_{sl}^+$). We conclude that a pair of colloids have to slide at least a distance l_{sl}^+ , before deterministically turning away, as the underlying mechanism for the CLF.

B. Effect of long-ranged translational repulsion

We now switch on χ_t and ask how the properties of the flock differ. On the $(l_r/b, l_t/b)$ plane, we find that there

is a clear region of flocking for non-zero χ_t (see Figure 3(a)). We further find that the flocks have crystalline order (see Figure 3(c),(e)). Such crystalline flocks in repulsive systems have been recently reported [26]. Similarly to the CLF, the CCF is destabilized by sufficiently high rotational torques. In addition, l_+ now is linear in l_t . l_+ being larger for a positive l_t , this thus renders a shorter sliding length for pair colloids during the CCF formation. The net result is thus a shorter sliding length compared to the CLF, which we can attribute to the difference between crystalline and liquid structures. We note that if this repulsion is too strong, the CCF is destabilized to a disordered gas (not shown here). The most generic form of the transition lines from the phase diagrams can be written as

$$l_r < l_+, \quad \frac{l_+}{b} = \frac{c_1}{\rho} + \frac{\beta_1 l_t}{b} \quad (8)$$

which is presented in Figures 1(a) and 3(a). We obtain β_1 and c_1 by first fitting the boundary line in Fig. 3(a). The slope gives $\beta_1 \approx 0.167$, whilst the x -intercept gives $c_1 \approx 0.013$. This c_1 then independently fixes the boundary on Fig. 1(a). We show in section IV how this can be derived from a continuum model of interacting density and polarization fields. The $\frac{c_1}{\rho}$ term inhibits sliding at high densities. We note that for densities above a critical density $\rho_c = (\frac{c_1}{b})^{2/3} \approx 0.05$, l_{sl} always exceeds the mean free path $\frac{1}{\sqrt{\rho}}$ so that flock formation can happen uninhibited. Thus, the destabilization at higher densities occurs as l_{sl}^- is approached due to the dominance of the instantaneous chemical sensing relative to the excluded volume repulsions (though in this regime collisions are more frequent). For $\chi_t > 0$, the second term further suppresses the sliding length due to long-ranged translational repulsion. Sliding over shorter distances effectively localizes particles in space and the effect is a crystalline structure.

We note that the flock destabilization mechanism here is independent of the contribution of noise. Though we have explicit noise terms in the updates in Eq.(1) for the sake of completion, they are set to be negligibly small (see Table I in Appendix). Indeed, if we were to define length scales $l_\eta = \frac{D_r b^2}{v_0}$ and $l_\xi = \frac{D_t}{v_0}$, using the values used of $D_r \approx 10^{-6}$ and $D_t \approx 10^{-8}$, we find that $l_\eta \sim 10^{-4}b$ and $l_\xi \sim 10^{-6}b$, thus negligible compared to all other length scales in the problem. We have repeated all the simulations presented in Fig. (1) with $D_r = D_t = 0$, and have found the results to be identical. Thus, as opposed to the conventional picture of noise induced inhibition of flock formation [4, 10, 21, 26] (i.e. deterministic alignment interactions compete with randomness in the same interaction channel), our mechanism reports a competition between a *deterministic* length scale due to sensing of chemical gradients l_r (also l_t) and other deterministic length scales of the problem.

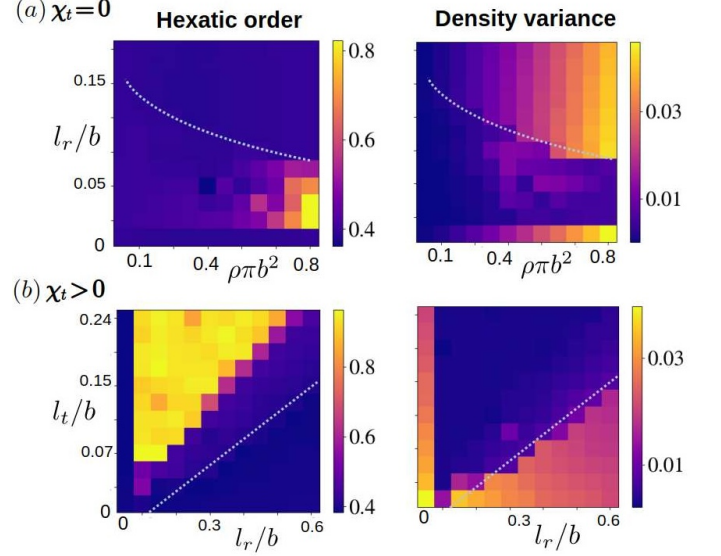


FIG. 4. Phase diagrams in terms of (left) global hexatic order (ψ_6) and (right) density variance. The panel on flocktop shows results for the case (a), which is $\chi_t = 0$ (CLF), whereas the bottom panel shows results for the case (b), which is $\chi_t > 0$ (CCF). Dotted curves indicate flocking order-disorder transition line. See text for details.

C. Difference between CCF and CLF

The difference in spatial structure between the CLF and CCF is readily distinguished by the pair correlation function $g(r) = \frac{1}{N} \sum_{i,j} \delta(r - |\mathbf{r}_i - \mathbf{r}_j|)$. This is plotted in Fig. (3)(f), distinguishing the solid and liquid signatures [25]. A closely related quantity [38] is the polar pair correlation $g(r, \phi)$ which explicitly depends on the orientations of the colloids. Here, $\cos(\phi_{ij}) = \mathbf{e}_i \cdot (\hat{\mathbf{r}}_i - \hat{\mathbf{r}}_j)$ [38]. For the CLF, we see that there are quadrants where neighbours are more likely to be found (3(d)), as opposed to the hexatic order of the CCF (3(e)). In the case of CCF, the intensity (proportional to the probability of finding the particle from the reference - see Appendix B) in the well-localized hexagonal positions of the crystal are substantially higher than in the CLF, which are instead less intense with a greater relative spread. The quadrant-like distribution indicate the repulsive torque-induced turn away of the particles in the forward and backward direction of the reference particle.

To further support the robustness of the mechanism, we report CLFs arising from repulsive torques with the addition of long-ranged *attractive* interactions, thus $\chi_t < 0$. We find that this phenomenology is maintained for $l_t \in [0, -0.01]$, before transitioning to a disordered gas for larger attractive translational interactions; this is shown in Figure 3(b). Putatively, the clumping tendency in this range is balanced by the excluded volume repulsions.

D. Hexatic order and density variance

We define a measure of local hexatic order ψ_i for the i th particle to quantify the hexatic order globally in terms of ψ_6 . They are given as [39]:

$$\psi_6 = \frac{1}{N} \sum_i \psi_i, \quad \psi_i = \frac{1}{N_i^n} \sum_j e^{i6\theta_{ij}}. \quad (9)$$

Here, θ_{ij} is the angle between particle i and particle j , and N_i^n is the number of neighbors for particle i ($N^n \approx 6$ for all data points). The observable ψ_6 is then averaged over 1000 different particle configurations at the steady-state. We plot ψ_6 for the two cases ($\chi_t = 0$ and $\chi_t > 0$) in the left panel of Fig. 4. The transition lines from the phase diagrams in Figures 1(a) and 3(a) are also shown as dotted lines for guide to the eye. In the case of $\chi_t = 0$ (Fig. 4(a) left), the hexatic order exists in the flocking phase, only for a very high density (area fraction $\rho\pi b^2 > 0.6$). Whereas, in case of $\chi_t > 0$ (Fig. 4(b) left), with $\rho\pi b^2 = 0.36$, the system becomes highly hexatic in the flocking phase. However, near the transition line, where density bands are prone to occur, the hexatic order gradually decreases.

Next, density variance for the two cases ($\chi_t = 0$ and $\chi_t > 0$) are shown in the right panel of Fig. 4. The density variance [15] is calculated from the density distribution for a specific parameter set shown in the phase diagram. For local density measurements, the Voronoi tessellation method has been implemented for a spatial configuration of particles. We calculate local density $\rho_l = \frac{\pi b^2}{A_l}$, where A_l is local area assigned to each particle. Then we compute the density variance as $\langle \rho_l^2 \rangle - \langle \rho_l \rangle^2$ (spatial average) and finally averaged over 1000 configurations. In both cases, the density variance is much lower in the flocking state. However, it shows an increase near the transition region. The density variance is high for the high area fraction ($\rho\pi b^2$) and in the disordered phase, for the case $\chi_t = 0$ (Fig. 4(a) right panel). For $\chi_t > 0$ case, with low χ_t values, the variance is more prominent, shown in Fig. 4(b) (right panel).

E. CCFs as solutions to equation of motion

Our choice of EOM in (1) is also unique in that it can be shown to support crystalline flocks as its dynamical fixed points. To see this, we firstly note that from the EOM the fixed points of θ_i are obtained by setting $\Omega_i = 0$, giving

$$\theta_i^* = \tan^{-1} \left(\frac{\sum_{j \neq i} (y_i - y_j) \prod_{k \neq i,j} |r_i - r_k|^3}{\sum_{j \neq i} (x_i - x_j) \prod_{k \neq i,j} |r_i - r_k|^3} \right) \quad (10)$$

The hexagonal lattice topology of CCF makes (10) tractable. Firstly, let us consider a hexagonal lattice

topology of distance $2b'$ aligned along the direction of the flock θ_i for the i th reference particle. To compute the sums in (10) one needs to evaluate the sums

$$\sum_j r_i - r_j = -b' \sum_{k=0}^K \sum_{n=1}^6 (1+k) \begin{pmatrix} \cos \left((n-1) \frac{\pi}{3} - \theta_i \right) \\ \sin \left((n-1) \frac{\pi}{3} - \theta_i \right) \end{pmatrix} \quad (11)$$

where K is the upper bound on the radial sums performed on the lattice; in our case $K = \frac{50}{b'} - 1$. For $\prod_{k \neq i,j} |r_i - r_k|^3$, we can evaluate this to be $\prod_{k=0}^K ((1+k)b')^{z-1} \delta_{k,j \in \{k\}} ((1+k)b')^z (1 - \delta_{k,j \in \{k\}})$, thus raised to power coordination number z minus one for the radial coordinate containing the j th particle (denoted by $j \in \{k\}$), and to the coordination number for all other radial coordinates. We recognize immediately that the symmetry of the lattice structure means that this depends on only the location of the “left out” particle j and the reference particle i . Without loss of generality, we label this product P_{ij} . The sums over n for each component in (11) can be readily computed by applying the double angle formulae and symmetries of the sine and cosine. The overall result is thus

$$\sum_j r_i - r_j = -b' \begin{pmatrix} \cos(\theta_i) \\ \sin(\theta_i) \end{pmatrix} S_K \quad (12)$$

where we have defined $S_K = \sum_{k=0}^K (1+k)$ (not needed to be evaluated explicitly). Thus the fixed point angle of (10) simply reads

$$\theta_i^* = \tan^{-1} \left(\frac{\sum_j (y_i - y_j) P_{ij}}{\sum_j (x_i - x_j) P_{ij}} \right) \quad (13)$$

which we see to be the self-consistent $\theta_i^* = \theta_i$ as required. Further, taking ratio of the coordinates of the positional dynamics at the fixed point, we see that $\frac{y_i}{x_i} = \tan(\theta_i)$ as required. We thus conclude that our particular choice of chemical interactions of (4) supports a crystalline flock. For fluid flocks the result is less trivial since various sums and products need to be weighted by an appropriate distribution function. We nevertheless see that enhanced fluctuations of θ_i^* is to be expected, since any approximate evaluation of (10) will contain various moments of each components of (11).

F. Order-disorder phase transition

We now present how polar order parameter $P = \langle |\mathbf{P}| \rangle_{ss}$ changes with variation of a control parameter l_r/b and l_t/b , shown in Fig. 5. First, for CLF ($l_t = 0$), phase transitions are shown for different densities of active particles, with area fraction $\phi = \rho\pi b^2$ (Fig. 5(a)). With zero l_r , $P \approx 0$ and there is no flocking (lower bound of Fig. 1(a)). As we increase l_r , particles flock into a polar ordered state. Whereas with further increase l_r ,

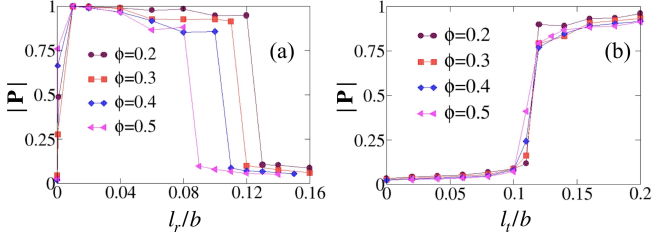


FIG. 5. Magnitude of the polar order parameter $|\mathbf{P}|$ versus l_r/b in panel (a) for the case of CLF. Here $l_t = 0$. In panel (b) we show, for the case of CCF, the variation of the order parameters as a function of l_t/b . Here, we have fixed $l_r = 0.55$. Different symbols indicates different area fraction $\phi = \rho\pi b^2$.

disordered phase are observed (see Fig. 1(a)). Transition points shift towards lower l_r/b values with increase of density. Then, for the CCF (with fixed $l_r = 0.55$), polar order parameter P versus l_t/b is plotted for different area fractions (for reference, see Fig. 4(b), where the area fraction is fixed at $\phi = 0.36$). In our model, the phase transition are highly dependent on the system size and many other parameters such as ρ , v_0 , χ_t and χ_r . Though of an first-order nature, an extensive study of the exact nature of the transition is left for future work. It needs to be noted that our model includes long-range interactions, and it is computationally expensive to work with such a system.

IV. CONTINUUM DESCRIPTION

In this section, we write the coarse-grained hydrodynamic equations for the density $\rho(\mathbf{r}, t)$ and polarization $\mathbf{p}(\mathbf{r}, t)$ fields by appealing to the symmetries and conservation laws of the system [39]. It is also possible to obtain these equations from well-established coarse-graining procedures [17, 38]. The continuum equations for our system can be written as:

$$\begin{aligned} \partial_t \rho &= -\nabla \cdot (v_{\text{tr}}(\rho) \mathbf{p} - D_{\text{tr}}(\rho) \nabla \rho) \\ \partial_t \mathbf{p} &= \Lambda(\rho) \frac{\nabla \rho}{2} + \frac{D_{\text{tr}}[\rho]}{\rho} [\nabla \cdot (\mathbf{p} \nabla \rho)] - D_r \mathbf{p} + D_t \nabla^2 \mathbf{p} \end{aligned} \quad (14)$$

Here, we have defined:

$$v_{\text{tr}} = v_0 - \chi_t \xi_0 \rho, \quad D_{\text{tr}} = \xi_t \rho \chi_t, \quad \Lambda = \xi_r \chi_r \rho - v_{\text{tr}} \rho$$

where the constants ξ_0 , ξ_t , and ξ_r are obtained by fitting the continuum model to the transition line predicted by the particle-based simulation in Fig. 1(a) and 3(a). From here on we set D_r , D_t terms to zero in (14) as they are negligibly small as explained in the previous section. In effect, the presence of these terms merely necessitate the formal coarse-graining procedure, but do not play any further role in explaining the instability of the flock.

We now proceed to study the stability of the flocking state. To this end, we linearize (14) about the steady-state density and polarizations (ρ^*, \mathbf{p}^*) , defining

$(\delta \rho, \delta \mathbf{p}) = (\rho - \rho^*, \mathbf{p} - \mathbf{p}^*)$. We use the following choice of Fourier basis expansion

$$\delta \tilde{\rho}(\mathbf{q}, \omega) = \int e^{i\mathbf{q} \cdot \mathbf{r}} e^{i\omega t} \delta \rho(\mathbf{r}, t) d^2 \mathbf{r} \quad (15a)$$

$$\delta \tilde{\theta}(\mathbf{q}, \omega) = \int e^{i\mathbf{q} \cdot \mathbf{r}} e^{i\omega t} (\nabla \cdot \delta \mathbf{p}) d^2 \mathbf{r} \quad (15b)$$

At the flocking state (ρ^*, \mathbf{p}^*) the following conditions hold: $\nabla \rho^* \rightarrow 0$ and $\nabla \cdot \mathbf{p}^* \rightarrow 0$. We now consider cases of $\chi_t = 0$ and $\chi_t > 0$ separately.

A. Case of $\chi_t = 0$

Here, we can solve equations (14) in real space; we obtain an enslaved dynamics of \mathbf{p} with respect to the density gradients:

$$\partial_t \mathbf{p} = \frac{\nabla \rho}{2} [(\chi_r \xi_r \rho - v_0)]. \quad (16)$$

We see that for the temporal evolution of \mathbf{p} to be stable with respect to the density gradients (feedback response), we require the following.

$$\chi_r < \frac{v_0}{\xi_r \rho^*}. \quad (17)$$

We see that the fluctuations in both ρ and \mathbf{p} are strongly coupled and that any fluctuations are stabilized in the long-time limit (see Appendix Fig. (7)).

B. General case with $\chi_t > 0$

Firstly, we may note that solving the $\mathbf{p} = 0$ in (14) gives $\rho^* = \frac{v_0}{\xi_r \chi_r + 2\xi_t \chi_t}$, a generalization of the above inequality. Further, we need to now linearize (14) in the bases of (15) to obtain the stability condition for the flocking state. The full linearization in Fourier space yields the following equation

$$\frac{d}{dt} \begin{pmatrix} \delta \tilde{\rho} \\ \delta \tilde{\theta} \end{pmatrix} = \begin{pmatrix} -q^2 \xi_t \chi_t \rho^* & -v_{\text{tr}}[\rho^*] \\ -\frac{q^2}{2} B[\rho^*] & 0 \end{pmatrix} \begin{pmatrix} \delta \tilde{\rho} \\ \delta \tilde{\theta} \end{pmatrix} \quad (18)$$

Here $B[\rho^*] = (2\xi_0 \chi_t + \xi_r \chi_r) \rho^* - v_0$. The dispersion relation for $\omega(q)$ then reads

$$\omega = \frac{iq^2 \xi_r \chi_t \rho^*}{2} \left[1 \pm \sqrt{1 + \frac{2v_{\text{tr}} q^2 B}{q^4 \xi_t^2 \chi_t^2 \rho^{*2}}} \right] \quad (19)$$

with the condition for long-wavelength instability given by:

$$2\xi_0^2 \rho^{*2} \chi_t^2 - \xi_0 \rho^* (2v_0 - \xi_r \chi_r \rho^*) \chi_t - v_0 (\xi_r \chi_r \rho^* - v_0) > 0$$

Using the above, we can solve for χ_t . The solution is:

$$\chi_t^* = \frac{v_0 - \frac{\xi_r \chi_r \rho^*}{2}}{2\xi_0 \rho^*} \left[1 \pm \sqrt{1 - \frac{2(\frac{\xi_r \chi_r \rho^*}{v_0} - 1)}{(1 - \frac{\xi_r \chi_r \rho^*}{2v_0})^2}} \right] \quad (20)$$

Let us consider the negative solution $\chi_t < \chi_t^*$. Let us further study the limit $\frac{\chi_r}{v_0} \ll 1$. Using the definitions for l_r and l_t , the desired inequality is thus

$$l_r^* \gtrsim \frac{2b}{\xi_r} \frac{1}{\rho^*} + \frac{2.73\xi_0 b^3}{\xi_r} l_t \quad (21)$$

We can identify this to have the same functional form as Eq.(8) defining the transition line. Equating with Eq. (8), we have that

$$c_1 = \frac{2}{\xi_r}, \quad \beta_1 = \frac{2.73\xi_0 b^3}{\xi_r} \quad (22)$$

We can thus infer the values of $\xi_r \approx 2c_1 \approx 0.026$ and $\xi_0 \approx 1.6 \times 10^{-3}$. We thus conclude that the noiseless limit of a minimal hydrodynamic model captures the destabilization transition of the flock. In addition, such transitions within between order/disorder phases (e.g. Fig. 3(b)) are also captured, although there is no explicit spatial-structure instability encoded in the hydrodynamic model (unlike for instance in [37]).

V. CONCLUSIONS

To conclude, we present a minimal mechanism for formation of fluid flocks that only requires long-ranged (net) repulsive torques and short-ranged repulsive forces from steric interactions. Although the roles of excluded volume interactions [15, 16, 19, 21], repulsive torques - either short [15] or long [26] ranged - and long-ranged repulsive forces [21, 26] have been studied separately, we have analyzed here the individual contributions of each of those components, and argued that the former two are the minimal requisite components. Our mechanism can be summarized as follows: the pair colloids slide together for at least a unit length before deterministically rotating away from each other. This is required to break the forward-backward symmetry at the pair-collision level. Destabilizing of the flock arises due to symmetric collisions at the pair colloidal level, wherein they slide exceedingly short before rotating away upon collision. These results we show to be consistent with a minimal hydrodynamic theory. One may ask whether such a sliding mechanism alone added to cognitive based (agent based) models [10, 11] could reproduce the flocking transition; indeed we will leave this to future work.

The CLF (or the polar liquids) are both generated by, and further destabilized by, the deterministic torques themselves. Notably, the apparent ubiquitous role of noise in destabilizing flocks [4, 10, 21, 26] is also absent in our mechanism (these are negligibly small in our simulation). We note that in the absence of short-ranged excluded volume repulsions, our results would converge to that recently studied in [26] where the need for (long-ranged) repulsive forces is more imminent. Translational

repulsion merely renders the flock to acquire a crystalline structure. We also have not studied here the role of particle shape anisotropy [14, 17], which would add additional competing length scales to our analysis. We expect our results here to be directly relevant to a variety of experimental systems. For example, migrating cell collections have been widely reported to exhibit spatial organization resembling a polar fluid [22, 28], while their interaction mechanism has been known to include (among others) long-ranged chemotaxis and avoidance torques [27]. The presented mechanism being very generic, we expect it to also be relevant for interacting colloids of non-chemical origin [25, 37, 38], where the underlying mechanism should also hold.

CONFLICTS OF INTEREST

There are no conflicts to declare.

DATA AVAILABILITY

The datasets are generated from simulation. They are available from the corresponding authors on reasonable request.

ACKNOWLEDGMENTS

We thank Professor Mike Cates for discussions. AGS acknowledges funding from the DIA Fellowship from the Government of India. SA acknowledges support from the National Postdoctoral Fellowship (SERB File number: PDF/2023/002096) provided by ANRF, Government of India. RS acknowledges support from seed and initiation grants from IIT Madras as well as a Start-up Research Grant from SERB (SERB File Number: SRG/2022/000682), India.

APPENDIX

Appendix A: Simulation details

The update equations is given in Eq. 1 of the main text. The position and orientations of the particles are updated using a forward Euler-Maruyama method. Initially particles are distributed randomly over the two-dimensional space. The initial orientations are also randomly distributed over the range of angles $[-\pi, +\pi]$ (angles are computed with respect to the positive x -axis). Periodic boundary conditions are applied on both the x -axis and y -axis. To compute chemical interactions using the expression of \mathbf{J}_i , we need to sum over periodic images. We have used a regular summation convention (using minimum image convention) for all results reported here, and checked these with the full Ewald summation

FIG	L	dt	b	v_0	κ	N	χ_t	χ_r	D_r	D_t
1	100	0.01	1	50	175	(319, 2578)	0	(0, 7)	10^{-6}	10^{-8}
3.(a)	100	0.01	1	50	175	1024	(0, 5)	(0, 10)	10^{-6}	10^{-8}
3.(b)	100	0.01	1	50	175	1024	(-1, 0)	(0, 10)	10^{-6}	10^{-8}
3.(d)	186	0.01	1	50	175	4000	0	0.75	10^{-6}	10^{-8}
3.(e)	186	0.01	1	50	175	4000	3	6	10^{-6}	10^{-8}
4.(a)	(77, 354)	0.01	1	50	175	1600	0	(0, 9)	10^{-6}	10^{-8}
4.(b)	118	0.01	1	50	175	1600	(0, 12)	(0, 32)	10^{-6}	10^{-8}
5.(a)	100	0.01	1	50	175	(637, 1592)	0	(0, 8)	10^{-6}	10^{-8}
5.(b)	100	0.01	1	50	175	(637, 1592)	(0, 10)	27	10^{-6}	10^{-8}

TABLE I. Parameter values used for respective figures of the paper. Here L is system size, b is the radius of the particle, N is the number of particles, dt is the time-stepping of the Euler-Maruyama integrator. The remaining parameters are defined after Eq.(1). Note that we consider noise to be less dominant to deterministic effects. Indeed, for the results in this paper, the Péclet number $Pe = v_0/(bD_r)$ is around 10^9 .

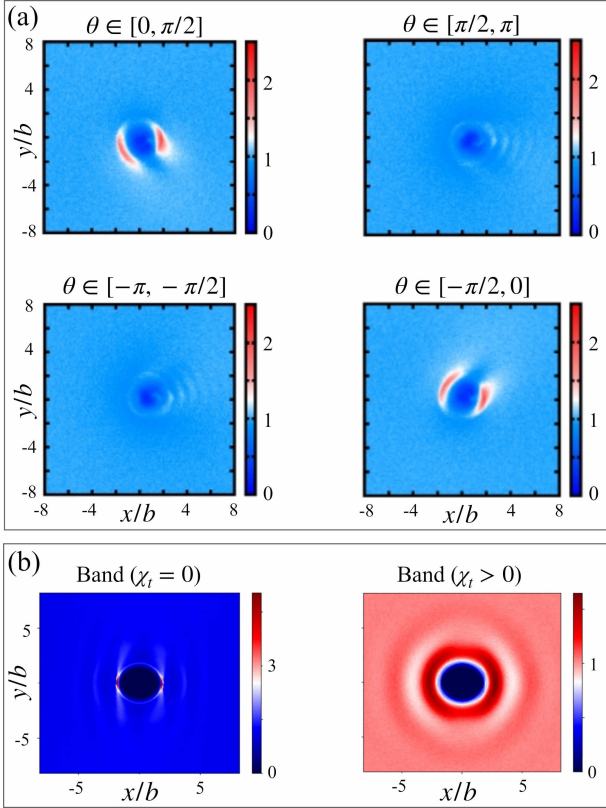


FIG. 6. Pair correlation function $g(r, \phi, \theta)$ for the isotropic phase for four different θ ranges in panel (a). Pair correlation function $g(r, \phi)$ in the band phase for $\chi_t = 0$ and $\chi_t > 0$ in (b).

convention for selected parameter values. A summary of all of the values of parameters used for the simulation are given in Table (I).

Appendix B: Correlation functions and fluctuations

The pair distribution function $g(r, \phi, \theta)$ implies correlations and provides the probability density of finding a pair of particles at a distance r with relative angles ϕ and θ . The angle ϕ is between the relative position r and the self-propulsion direction of the tagged particle, $\hat{\mathbf{e}}_i \cdot \hat{\mathbf{r}}_{ij} = \cos \phi$ and θ is the angle between the propulsion directions of the particle pair. To obtain this pair distribution function, histograms are created with the number of particles $N_h(r, \phi, \theta)$ at distance r , positional angle ϕ and relative angle θ . The bins are chosen as $0.1b$ for r , $\pi/150$ for ϕ and $\pi/2$ for θ . Then we need to normalize $N_h(r, \phi, \theta)$, to obtain the pair distribution function $g(r, \phi, \theta)$. The number of configurations is $t_c(10000)$ snapshots, over which histograms are made. The area of the annular segment of radial width dr , angular width $d\phi$ is given by $A_r = r dr d\phi$. The number density is $\rho = N/L^2$ and the size of the relative orientation bin is $d\theta$. Then the normalization factor is $N_r = \frac{A_r \rho N t_c d\theta}{2\pi}$ and the pair distribution function is given by $g(r, \phi, \theta) = N_h(r, \phi, \theta)/N_r$.

An example of this for isotropic phase is given in Fig. 6(a). The pair distribution functions are determined for the four different θ ranges as: $\theta: [0, \pi/2]$, $\theta: [\pi/2, \pi]$, $\theta: [-\pi, -\pi/2]$ and $\theta: [-\pi/2, 0]$. We see that in the isotropic phase, the probability of finding a neighboring particle is different in the front relative to the back of the direction of motion (orientation), indicative of the symmetry breaking in an active disordered gas [17, 26, 38]. In the main text, we show that $g(r, \phi)$ also distinguishes CLFs from CCFs, the former having a more quadrant-like structure compared to the latter's hexatic structure. In addition, we compare the structure of $g(r, \phi)$ for the band phases in Fig. (6)(b), for the CLF and CCF density bands. Note that the band structure is more dense in the case of $\chi_t = 0$, resulting a more intense correlation in $g(r, \phi)$. A related quantity that we compute is the radial $g(r)$, given by

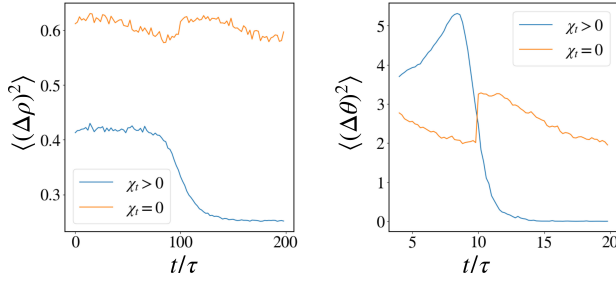


FIG. 7. Comparison of CLF ($\chi_t = 0$) and CCF ($\chi_t > 0$) via density fluctuations ($\langle(\Delta\rho)^2\rangle$), and orientational fluctuations ($\langle(\Delta\theta)^2\rangle$). For the CLF, the panel on the left shows residual fluctuations, whereas for the CCF, the fluctuations die out in the steady-state. In the panel on the right, a similar phenomenon is seen for the orientational fluctuations. Note that both curves are strongly correlated (shared monotonicity).

$$g(r) = \frac{1}{N} \sum_{i,j} \langle \delta(|\mathbf{r}_i - \mathbf{r}_j| - r) \rangle \quad (\text{B1})$$

this is plotted in Fig. (3), distinguishing the CLF and CCF.

An additional feature of the CLF is that they have a steady-state persistent fluctuations of both density and polarization fields (dynamical steady-state - note that our simulations are effectively noiseless), which is absent in the CCF. In Fig.7, we show fluctuations for positions and orientations for CLF and CCF. Here, the Density fluctuations is given by: $\langle(\Delta\rho)^2\rangle = \langle\rho^2\rangle - \langle\rho\rangle^2$. Here, $\langle \rangle$ denotes a spatial average. Note that the ρ field has to be obtained via binning. We also measure Orientational (angular) fluctuations, which is given by $\langle(\Delta\theta)^2\rangle = \langle\theta^2\rangle - \langle\theta\rangle^2$. Here, $\langle \rangle$ denotes average over colloids.

Appendix C: Description of the supplementary movies

The time evolution of the CCF and CLF structures for a larger system with total number of particles $N = 20000$, are attached as supplementary movies [29]. We note that our results are robust as we change number of particles in the simulations. For both cases, we started with random initial conditions (positions and orientations), and update the equation of motion following Eq. 1. In both movies, the particles are colored by their orientations (given in terms of the angle θ their orientation vector makes with the positive x -axis). The color bar is same as the one used in Fig. 1. Two particles are intentionally colored black throughout the simulation to simply trace them during the dynamics. Polar order or the flocking state collectively emerges in this model with both the cases. Parameters used for the two movies are below.

- **Movie I.** In the case of $\chi_t = 0$ (CLF), the liquid flock gradually forms throughout the system and moves in a particular direction. The fixed parameter values are: $L = 418$, $b = 1$, $dt = 0.01$, $D_r = 10^{-3}$, $D_t = 10^{-3}$, $\kappa = 175$, $v_0 = 50$, $\chi_t = 0$, $\chi_r = 0.75$.
- **Movie II.** In the case of $\chi_t > 0$ (CCF), the particles first start to form local polar flocks (colored patch), then merge and pick a particular direction of motion entirely. The fixed parameter values are: $L = 418$, $b = 1$, $dt = 0.01$, $D_r = 10^{-3}$, $D_t = 10^{-3}$, $\kappa = 175$, $v_0 = 50$, $\chi_t = 3$, $\chi_r = 6$.

-
- [1] J. Toner, *The Physics of Flocking: Birth, Death, and Flight in Active Matter* (Cambridge University Press, 2024).
 - [2] I. D. Couzin, J. Krause, R. James, G. D. Ruxton, and N. R. Franks, Collective memory and spatial sorting in animal groups, *Journal of theoretical biology* **218**, 1 (2002).
 - [3] T. Vicsek, A. Czirók, E. Ben-Jacob, I. Cohen, and O. Shochet, Novel type of phase transition in a system of self-driven particles, *Physical review letters* **75**, 1226 (1995).
 - [4] H. Chaté, F. Ginelli, G. Grégoire, and F. Raynaud, Collective motion of self-propelled particles interacting without cohesion, *Physical Review E—Statistical, Nonlinear, and Soft Matter Physics* **77**, 046113 (2008).
 - [5] J. Toner, Y. Tu, and S. Ramaswamy, Hydrodynamics and phases of flocks, *Annals of Physics* **318**, 170 (2005).
 - [6] J. Toner, Birth, death, and horizontal flight: Malthusian flocks with an easy plane in three dimensions, *Phys. Rev. E* **110**, 064604 (2024).
 - [7] H. Ikeda, Minimum scaling model and exact exponents for the nambu-goldstone modes in the vicsek model, *Physical Review Letters* **133**, 258301 (2024).
 - [8] H. Chaté and A. Solon, Dynamic scaling of two-dimensional polar flocks, *Physical Review Letters* **132**, 268302 (2024).
 - [9] P. Jentsch and C. F. Lee, New universality class describes vicsek's flocking phase in physical dimensions, *Physical Review Letters* **133**, 128301 (2024).
 - [10] S. Adhikary and S. Santra, Pattern formation and phase transition in the collective dynamics of a binary mixture of polar self-propelled particles, *Physical Review E* **105**, 064612 (2022).
 - [11] S. Adhikary and S. Santra, Collective dynamics and phase transition of active matter in presence of orientation adapters, *arXiv preprint arXiv:2302.13035* (2023).
 - [12] P. Baconnier, O. Dauchot, V. Démery, G. Düring, S. Henkes, C. Huepe, and A. Shee, Self-aligning polar active matter, *Reviews of Modern Physics* **97**, 015007 (2025).

- [13] M. E. Cates and C. Nardini, Active phase separation: new phenomenology from non-equilibrium physics, *Reports on Progress in Physics* **88**, 056601 (2025).
- [14] H. Wensink and H. Löwen, Emergent states in dense systems of active rods: from swarming to turbulence, *Journal of Physics: Condensed Matter* **24**, 464130 (2012).
- [15] M. Knežević, T. Welker, and H. Stark, Collective motion of active particles exhibiting non-reciprocal orientational interactions, *Scientific Reports* **12**, 19437 (2022).
- [16] L. Chen, K. J. Welch, P. Leishangthem, D. Ghosh, B. Zhang, T.-P. Sun, J. Klukas, Z. Tu, X. Cheng, and X. Xu, Molecular chaos in dense active systems, *arXiv preprint arXiv:2302.10525* (2023).
- [17] R. Großmann, I. S. Aranson, and F. Peruani, A particle-field approach bridges phase separation and collective motion in active matter, *Nature communications* **11**, 5365 (2020).
- [18] J. Chen, X. Lei, Y. Xiang, M. Duan, X. Peng, and H. Zhang, Emergent chirality and hyperuniformity in an active mixture with nonreciprocal interactions, *Physical Review Letters* **132**, 118301 (2024).
- [19] A. Martín-Gómez, D. Levis, A. Díaz-Guilera, and I. Pagonabarraga, Collective motion of active brownian particles with polar alignment, *Soft matter* **14**, 2610 (2018).
- [20] E. Sese-Sansa, I. Pagonabarraga, and D. Levis, Velocity alignment promotes motility-induced phase separation, *Europhysics Letters* **124**, 30004 (2018).
- [21] L. Caprini and H. Löwen, Flocking without alignment interactions in attractive active brownian particles, *Physical Review Letters* **130**, 148202 (2023).
- [22] T. Hiraiwa, Dynamic self-organization of idealized migrating cells by contact communication, *Physical Review Letters* **125**, 268104 (2020).
- [23] M. Kumar, A. Murali, A. G. Subramaniam, R. Singh, and S. Thutupalli, Emergent dynamics due to chemohydrodynamic self-interactions in active polymers, *Nature Commun.* **15**, 4903 (2024).
- [24] A. G. Subramaniam, M. Kumar, S. Thutupalli, and R. Singh, Rigid flocks, undulatory gaits, and chiral foldamers in a chemically active polymer, *New Journal of Physics* **26**, 083009 (2024).
- [25] A. Bricard, J.-B. Caussin, N. Desreumaux, O. Dauchot, and D. Bartolo, Emergence of macroscopic directed motion in populations of motile colloids, *Nature* **503**, 95 (2013).
- [26] S. Das, M. Ciarchi, Z. Zhou, J. Yan, J. Zhang, and R. Alert, Flocking by turning away, *Physical Review X* **14**, 031008 (2024).
- [27] B. A. Camley and W.-J. Rappel, Physical models of collective cell motility: from cell to tissue, *Journal of physics D: Applied physics* **50**, 113002 (2017).
- [28] M. Hayakawa, T. Hiraiwa, Y. Wada, H. Kuwayama, and T. Shibata, Polar pattern formation induced by contact following locomotion in a multicellular system, *Elife* **9**, e53609 (2020).
- [29] See the supplemental material at this URL: [to be inserted].
- [30] B. V. Hokmabad, J. Agudo-Canalejo, S. Saha, R. Golestanian, and C. C. Maass, Chemotactic self-caging in active emulsions, *Proc. Natl. Acad. Sci.* **119**, e2122269119 (2022).
- [31] S. Saha, R. Golestanian, and S. Ramaswamy, Clusters, asters, and collective oscillations in chemotactic colloids, *Phys. Rev. E* **89**, 062316 (2014).
- [32] R. Soto and R. Golestanian, Self-assembly of active colloidal molecules with dynamic function, *Phys. Rev. E* **91**, 052304 (2015).
- [33] G. Rückner and R. Kapral, Chemically powered nanodimers, *Physical review letters* **98**, 150603 (2007).
- [34] R. Singh, R. Adhikari, and M. Cates, Competing chemical and hydrodynamic interactions in autophoretic colloidal suspensions, *The Journal of chemical physics* **151** (2019).
- [35] Indeed, the polar order is expected to be destroyed at larger values of fluctuations [3]. In this paper, we choose noise to be less dominant to deterministic effects by choosing Péclet number $Pe = v_0/(bD_r)$ to be around 10^9 .
- [36] D. Geyer, A. Morin, and D. Bartolo, Sounds and hydrodynamics of polar active fluids, *Nature materials* **17**, 789 (2018).
- [37] D. Geyer, D. Martin, J. Tailleur, and D. Bartolo, Freezing a flock: Motility-induced phase separation in polar active liquids, *Physical Review X* **9**, 031043 (2019).
- [38] J. Zhang, R. Alert, J. Yan, N. S. Wingreen, and S. Granick, Active phase separation by turning towards regions of higher density, *Nature Physics* **17**, 961 (2021).
- [39] P. M. Chaikin, T. C. Lubensky, and T. A. Witten, *Principles of condensed matter physics*, Vol. 10 (Cambridge university press Cambridge, 1995).